Title: Single-cell characterization of peripheral blood mononuclear cells from Crohn's disease patients on vedolizumab

Short title: PBMC characterization of CD patients on VDZ

Andrew Y.F. Li Yim[1,2,3,4,5,9,*], Ishtu L. Hageman[1,2,3,*], Vincent Joustra[2,3,*], Ahmed Elfiky[1,2,4], Mohammed Ghiboub[1,2,5,11], Evgeni Levin[8,9], Jan Verhoeff[1,2,10,11,12], Caroline Verseijden[1], Iris Admiraal-van den Berg[1], Marcel M.A.M. Mannens[6,7], Marja E. Jakobs[6], Susan B. Kenter[6], Alex T. Adams[13], Jack Satsangi[13], Geert R. D'Haens[2,3], Wouter J. de Jonge[1,2,3,14,†], and Peter Henneman[2,6,7,11]

[1]Tytgat Institute for Liver and Intestinal Research, Amsterdam UMC location University of Amsterdam, Amsterdam, Netherlands.
[2]Amsterdam Gastroenterology Endocrinology Metabolism, Amsterdam, Netherlands
[3]Department of Gastroenterology and Hepatology, Amsterdam UMC location University of Amsterdam, Amsterdam, Netherlands
[4]Center for Translational Immunology, University Medical Centre Utrecht, Utrecht University, Utrecht, Netherlands
[5]Emma Children's Hospital, Pediatric Surgery, Amsterdam UMC location University of Amsterdam, Amsterdam, Netherlands
[6]Genome Diagnostics Laboratory, Department of Human Genetics, Amsterdam UMC location University of Amsterdam, Amsterdam, Netherlands.
[7]Amsterdam Reproduction and Development, Amsterdam, Netherlands
[8]Department of Vascular Medicine, AmsterdamUMC location University of Amsterdam, Amsterdam, Netherlands
[9]Horaizon BV, Delft, Netherlands
[10]Department of Molecular Cell Biology and Immunology, Amsterdam UMC location Free University of Amsterdam, Amsterdam, Netherlands.
[11]Amsterdam Infection & Immunity, Amsterdam, Netherlands
[12]Cancer Center Amsterdam, Amsterdam, Netherlands
[13]John Radcliffe Hospital, Translational Gastroenterology Unit, Oxford, United Kingdom.
[14]Department of Surgery, University of Bonn, Bonn, Germany.
*Equally contributing first authors.
[†]Equally contributing senior authors.

Grant support: This work was in part funded by the Helmsley Trust Foundation.

Corresponding author: Andrew Y.F. Li Yim
Email: a.y.liyim@amsterdamumc.nl

Authors contributions:

Conduction of the study, laboratory, and writing of the manuscript: ALY, IH; study design: ALY, IH, VJ, WJ, PH; single-cell RNA-sequencing and analysis: ALY, IH, MJ, SK; mass cytometry analyses: JV, IH, ALY; flow cytometry analyses: ALY, IH, AE, CV, IAB; bulk RNA-sequencing and analysis: ALY, IH, AE, MJ; bioinformatics analysis: ALY, JV; patients samples collection: VJ, IH; sample preparation: IH, MG; supervision: PH, WJ, GD; reviewing and editing: WJ, GD, PH, EL, JS, AA, MM. All authors have read and agreed to the published version of the manuscript.

This work has been published as part of a thesis [1].

Abstract

Background & Aims. Vedolizumab (VDZ) is a monoclonal antibody approved for the treatment of Crohn's disease (CD) by abrogating the gut-homing behavior of various leukocytes. Despite its efficacy, non-response to VDZ is common in clinical practice. Here, we performed an observational case-control study to interrogate the differences between responders and non-responders to VDZ during treatment.

Methods. CD patients on VDZ treatment were classified as steroid-free responder or non-responder based on endoscopic- (≥3 drop in Simple Endoscopic Score for Crohn's Disease (SES-CD)), biochemical (≥50% reduction in C-reactive protein (CRP) and fecal calprotectin) and/or clinical response criteria (≥3 point drop in Harvey-Bradshaw Index (HBI)) during which peripheral blood was collected. Peripheral blood mononuclear cells (PBMCs) were isolated from a cohort of four responders and four non-responders which were then subjected to single-cell RNA-sequencing (scRNAseq) and mass cytometry by time of flight (CyTOF) analyses.

Results. The most prominent differences between responders and non-responders were observed in the T and myeloid compartment, which were more and less abundant, respectively, among non-responders. T cells from non-responders generally presented lower expression of inhibitors of the NFκB signaling pathway. Abundance-wise, a lower concentration of plasmacytoid dendritic cells (pDCs) was observed among non-responders, which could be correlated with a higher abundance of pDCs in lesional tissue based on a public dataset. Classical monocytes presented an different transcriptome, with non-responders presenting lower expression of genes involved in wound-healing and cytokine-cytokine receptor signaling.

Conclusions. Non-response to VDZ during treatment is associated with differences in abundance and expression of the T and myeloid compartment.

Keywords: single-cell RNA-sequencing, scRNAseq, cytometry by time of flight, CyTOF, vedolizumab, therapy response, T cell, pDC, classical monocytes.

Introduction

Crohn's disease (CD) is an incurable, chronic, inflammatory condition of the gastrointestinal tract characterized by a relapsing-remitting transmural inflammation of the digestive tract belonging to the family of inflammatory bowel diseases (IBD). Current treatments for CD include the use of monoclonal antibodies that target mediators of inflammation with the goal of ameliorating the inflammatory phenotype and/or maintaining a state of clinical and endoscopic remission. One such monoclonal antibody is vedolizumab (VDZ), which was approved for use in CD patients in 2014 by the United States Food and Drug Administration as well as the European Medicines Agency [2].

VDZ targets the gut homing receptor complex integrin $\alpha_4\beta_7$ (also known as lymphocyte Peyer's patch adhesion molecule 1; LPAM-1) [3,4], which prevents it from binding mucosal vascular addressin cell adhesion molecule 1 (MAdCAM-1), a molecule expressed exclusively by the intestinal endothelial cells. By preventing integrin $\alpha_4\beta_7$ from binding MAdCAM-1, the attachment and stabilization of circulating immune cells that express integrin $\alpha_4\beta_7$ to high endothelial venules in the gut is destabilized, thereby abrogating gut-homing capabilities [5–7]. While VDZ has traditionally been discussed within the context of the T cell lineage [8–11], more recent studies suggest that the myeloid [12,13] as well as B cells [14] are affected by VDZ treatment as well. Despite the advances VDZ therapy has provided patient care, the efficacy or therapy response rate is reported to be approximately between 30% to 45% [2,15–17] with a recent meta-analysis indicating that loss of response towards VDZ among CD patients was estimated at 47.9 per 100 person-years [18]. To date, we have no proper understanding why only a subgroup of patient responds to therapy, nor do we have a prognostic biomarker for predicting response to VDZ therapy. To better understand how response to VDZ manifests, we conducted an exploratory case-control study to characterize the immune cell composition of peripheral blood mononuclear cells (PBMCs) from CD patients on VDZ treatment. Here, we compared the composition between responders and non-responders using single-cell RNA-sequencing (scRNAseq) and cytometry by time of flight (CyTOF).

Methods

Sample collection and preparation

Blood samples were obtained from patients included in the EPIC-CD study, which is a multi-center consortium with the goal of identifying prognostic biomarkers at the level of peripheral blood (PBL) DNA methylation capable of predicting response to adalimumab, infliximab, vedolizumab, and ustekinumab prior to treatment in CD patients [19]. For the current study, 8 VDZ-treated CD patients (4 responders and 4 non-responders) were sampled for peripheral blood at a median of 26 weeks into treatment during routine care at the AmsterdamUMC hospital, location AMC, Amsterdam, Netherlands (**Table 1**). Patients were labeled as steroid-free responder to VDZ if they had measurable drug concentrations in serum and presented endoscopic- (≥3 drop in Simple Endoscopic Score for Crohn's Disease (SES-CD)), biochemical (≥50% reduction in C-reactive protein (CRP) and fecal calprotectin), and/or clinical response criteria (≥3 point drop in Harvey-Bradshaw Index (HBI)) relative to their baseline measurements. Immediately after collecting peripheral blood, peripheral blood mononuclear cells (PBMC) were isolated by means of Ficoll (GE Healthcare) separation and IMDM medium (Gibco) supplemented with 10% DMSO and 50% FBS (Serana). Isolated PBMCs were stored overnight at -80 C in Mr. Frosty freezing containers (Thermo) where after they were transferred to liquid nitrogen until cohort completion.

Single-cell RNA-sequencing analysis

Samples were removed from the cryostat and thawed on ice. Thawed PBMCs were washed and then labelled using the hashtag oligo (HTO) antibodies for multiplexing purposes whereupon the oligo-tagged PBMC suspensions were then mixed and distributed across 6 GEM-wells on the Chromium controller (10X Genomics). Single-cell barcoded partitions were prepared using 10X chemistry v3 where after separate sequencing libraries were prepared for HTOs and the actual mRNA after size-selection. Libraries were sequenced on the Illumina HiSeq4000 in a 150 bp paired-ended fashion at the Core Facility Genomics, Amsterdam UMC. The mRNA libraries were sequenced on 150M reads per GEM-well, whereas the HTO libraries were sequenced to a depth of 50M reads per GEM-well. Raw data was imported and analyzed in R. A detailed overview as well as the data analyses can be found in the **Supplementary Information**.

Mass cytometry by time-of-flight

Concurrent with the single-cell RNA-sequencing analyses, mass cytometry by time of flight (CyTOF) was performed on a separate aliquot of the PBMC samples. Here, we measured the cell-surface expression of 37 proteins with a particular focus on the T cell lineage. Acquisition was performed on the Fluidigm Helios system. Sample was diluted in H_2O and

supplemented with 10% v/v of EQ Four Element Calibration beads (Fluidigm). Staining, barcoding, data acquisition, and analyses were performed in R and are described in **Supplementary Information**. An overview of all the antibodies used and their clones can be found in **Supplemental Table 1**.

Flow cytometry of the plasmacytoid dendritic cells

In addition to using an aliquot of PBMCs of the same patients analyzed for scRNAseq and CyTOF, an additional two patients (1 responder and 1 non-responder) were included in the flow cytometry analyses. Upon thawing, PBMCs were washed in PBS and stained for a live/dead cell viability marker (LifeScience, Amsterdam, the Netherlands). Cells were subsequently stained for surface markers in FACS buffer (0.5% BSA, 0.01% NaN3 in PBS) using the following antibodies: CD11c-PerCP Cy5.5 (clone: S-HCL-3, BioLegend), HLA-DR-Alexa Fluor 700 (clone: LN3, eBioscience), CD123-FITC (clone: 6H6, BioLegend), CD1C-PE-Cy7 (clone: L161, BioLegend), pan-lineage (CD3/CD19/CD20/CD56)-APC (clones: UCHT1;HIB19;2H7;5.1H11, BioLegend), CD14-BD Horizon V500 (clone: M5E2, Becton Dickinson) and CD16-PE (clone: 3G8, Becton Dickinson). Acquisition was performed on the BD LSR Fortessa™, where plasmacytoid DCs (pDCs) were identified as (T/B/NK)Lin$^-$HLA-DR$^+$CD14$^-$CD16$^-$CD11c$^-$CD123$^+$. Analysis was performed using FlowJo (Treestar) and R. The gating strategy can be found in the **Supplementary Information.** An overview of all antibodies and their clones used can be found in **Supplemental Table 2**.

RNA-sequencing of the classical monocytes

Akin to the flow cytometric analyses, PBMCs were washed in PBS and stained for a live/dead cell viability marker (LifeScience, Amsterdam, the Netherlands) alongside the antibodies mentioned above. Cell sorting was conducted on the SH800 Cell Sorter (Sony). Classical, intermediate, and non-classical monocytes were identified as (T/B/NK)Lin$^-$HLA-DR$^+$CD14^{++}CD16$^-$, HLA-DR$^+$CD14^{++}CD16$^+$, and HLA-DR$^+$CD14$^+$CD16$^+$, respectively. The classical monocytes were sorted out and were subsequently processed for RNA sequencing. Due to low input material, classical monocytes mRNA was converted into cDNA using the Ovation RNA-seq System V2 kit (NuGEN; Agilent, Santa Clara, United States), whereupon sequencing libraries were prepared using the Ovation Ultralow System V2 kit (NuGEN; Agilent, Santa Clara, United States) and thereafter sequenced in a 150 bp paired-ended fashion on the Illumina NovaSeq6000 to a depth of 40 million reads at the Amsterdam UMC Core Facility Genomics. The data analyses can be found in the **Supplementary Information**.

Results

Cohort assembly

CD patients on VDZ treatment were followed at the AmsterdamUMC, location AMC as part of routine care. All included patients provided informed consent and the sampling was in accordance with the institutional ethics committee (METC reference number: NL53989.018.15). Response to treatment in the EPIC-CD consortium was defined as endoscopic- (≥50% drop in simple endoscopic score for Crohn's Disease (SES-CD)) in combination with biochemical (≥50% reduction in C-reactive protein (CRP) and fecal calprotectin or an absolute CRP < 5.0 µg/g and fecal calprotectin < 250 µg/g) and/or clinical response (≥3 point drop in Harvey-Bradshaw Index (HBI)) in the presence of measurable drug serum concentrations and in the absence of corticosteroid usage. For this study, we selected a cohort of 8 CD patients at a median of 14 weeks into VDZ treatment, which were classified as responder (N = 4) and non-responder (N = 4) (**Methods**, **Table 1**, and **Figure 1**).

ITGA4 expression detected on all PBMCs

Single-cell RNA-sequencing (scRNAseq) and mass cytometry by time of flight (CyTOF) provided transcriptional and proteomic profiles of 15,981 and 16,000 (subsampled from 1,783,641) cells, respectively. Cells were annotated to 31 known cell types (**Figure 2A-B**) using a combination of automatic and manual curation based on canonical markers (**Figure 2C-D**). We observed general agreement between the two experiments (r = 0.73; **Figure 2E**). Interrogation of the of the protein expression of integrin α_4 as well as its encoding gene *ITGA4* were measurably expressed in all cell types (**Figure 2F-G**)**.** By contrast, gene expression of *ITGB7* was notably muted, with the plasma cells presenting the highest expression. Nonetheless, our observations confirm that genes encoding integrin $\alpha_4\beta_7$ expression are active in many cell types and is hence not solely restricted to the T cells.

Circulating T cells from VDZ non-responders express lower levels of inhibitors of the NFκB signaling pathway

Differential abundance analysis of both the scRNAseq and CyTOF data indicated concordant differences between responders and non-responders (**Figure 3A-C** and **Supplemental Table 3**). Overall, we observed a significantly lower and higher concentration of myeloid (*p*-value = 4.6E-03) and T cells (*p*-value = 0.029), respectively, among the non-responders (**Figure 3D**). At a more granular level, a significantly higher proportion of CD8 T central memory (CD8 TCM) was observed through CyTOF (*p*-value = 0.01), which we could reproduce in direction, but not in significance, through scRNAseq (*p*-value = 0.89) (**Figure 3E**). At scRNAseq level, a significantly higher and lower proportion was observed for the mucosal associated invariant T cells (MAIT; *p*-value = 0.029) (**Figure 3F**) and plasmacytoid dendritic cells (pDCs; *p*-value = 0.041) (**Figure 3G**), respectively, which we were unable to reproduce using CyTOF as no markers were included for either MAIT or pDCs. As VDZ binds T cells in particular [8], we investigated whether their transcriptome presented response-associated differences (**Supplemental Table 4**). We specifically interrogated *ITGA4* and *ITGB7* expression but found no differences in expression for *ITGB7*. By contrast, *ITGA4* was found to be significantly higher in non-responders when looking at CD4 TEM, CD4 Treg, CD8 TCM, and CD8 TEM (**Figure 3H)**. Notably, we observed for multiple T cell subsets that genes encoding inhibitors of the NFκB signaling pathway, such as *TNFAIP3* and *NFKBIA*, were significantly lower in expression amongst non-responders (**Figure 3H**).

VDZ non-responders present higher concentrations of circulating plasmacytoid dendritic cells

As our CyTOF panel did not include markers for pDCs, we conducted flow cytometry analyses where we identified the (T/B/NK)Lin$^-$HLA-DR$^+$CD11c$^-$CD123$^+$ fraction (**Figure 4A**). Indeed, we observed a significantly lower proportion of circulatory pDCs among responders relative to the non-responders (**Figure 4B**). Comparing the transcriptome of responders with non-responders revealed no statistically significant response-associated differences after correcting for multiple testing (**Figure 4C** and **Supplemental Table 5**). However, interrogating the expression of *ITGA4* and *ITGB7* specifically indicated a notably lower expression of *ITGB7* amongst non-responders albeit statistically non-significant (*p*-value = 0.32) (**Figure 4D** and **Supplemental Table 5**). We hypothesized that the diminished circulatory pDC concentration among non-responders was due to the recruitment of pDCs into the gastrointestinal tract thereby removing them from circulation. To corroborate our hypothesis, we interrogated the publicly available single-cell transcriptomic data from CD patients' intestinal biopsies extracted from ileal lesions (involved) and adjacent non-lesional (uninvolved) tissue as published by Martin *et al.* [39]. Upon identifying the pDC fraction (**Figure**

4E), we found that the pDC proportion relative to the total immune fraction was suggestively higher in lesional compared to non-lesional areas (*p*-value = 0.067) (**Figure 4F**), indicating that the concentration pDCs are higher under inflammatory conditions, thereby supporting our hypothesis.

Classical monocytes from VDZ non-responders present an altered transcriptome.

UMAP visualization of the monocytes indicated response-associated clustering (**Figure 5A**), which was most visible for the classical monocytes, suggesting transcriptome-wide differences. Differential expression analysis of the classical monocytes identified 30 statistically significant differentially expressed genes (DEGs) (**Figure 5B** and **Supplemental Table 6**). Notably, responders presented higher expression of several monocyte/macrophage-function related genes including genes encoding cytokines (CXCL2 [40,41], CCL3 [42–44], CCL4 [45,46]), mediators of host defense signaling (RIPK2 [47]), and macrophage scavenging receptor (MSR1 [48]), typically observed in M2-like macrophages. By contrast, complement factor D encoding gene *CFD* and negative regulator of NFκB signaling pathway *VSTM1* [49] were higher among non-responders (**Figure 5C**). We were able to confirm differential expression for *CFD* and *MSR1* through bulk RNA-sequencing on sorted classical monocytes (**Figure 5D** and **Supplemental Table 7**). Specifically interrogating *ITGA4* and *ITGB7* indicated neither significant nor visible differences in the gene expression thereof (**Figure 5E**). Gene set enrichment analysis against the KEGG database identified general lower expression of the cytokine-cytokine receptor signaling pathway among non-responders (**Figure 5F-G** and **Supplemental Table 8**). We were therefore interested in identifying which other PBMCs were the sender/receiver to the differentially expressed cytokines produced by the classical monocytes. Among classical monocytes derived from responders, we observed a significantly higher expression of vascular endothelial growth factor (VEGF). Notably, VEGF receptor 1-encoding *FLT1* was found to be higher in both the CD4T naïve as well as the classical monocytes (**Figure 5H**), suggesting a more wound-healing phenotype in classical monocytes obtained from responders.

Discussion

We demonstrate that VDZ-treated CD patients differ in cellular composition and intrinsic cellular behavior when comparing responders with non-responders. Interrogating the T cell compartment suggested a higher abundance of MAIT and CD8 TCM among non-responders. Notably, both T cells from non-responders appeared to be transcriptionally primed for NFκB signaling, a signaling pathway typically reserved for inflammation, by downregulating inhibitors thereof. The priming of the NFκB pathway would match the non-responding

phenotype, where inflammation is still present despite treatment. While our results confirm that response to VDZ affects the T cell compartment, we also find response-associated differences within the myeloid compartment. We observed that the circulatory pDCs were less abundant amongst non-responders. The pDC population represents a unique cell type whose ontogeny and lineage affiliation remain under debate due to its similarity to both myeloid and lymphoid lineages [50–54]. Previously, pDCs were called "natural interferon producing cell" as they can produce large amounts of type I interferons (IFN), which typically occurs in response to viruses. This in turn activates NK and B cells [55–58], thereby bridging the innate and adaptive immune system. Remarkably, pDCs constitute only 0.4% of all measured cells when looking at all measured PBMCs in our scRNAseq experiment and only 0.12% of the immune compartment when interrogating ileal tissue from Martin *et al.* [39]. Despite the rarity of this cellular population, they have been implicated in multiple immune-mediated inflammatory disorders (IMIDs) [54]. Currently, an ongoing phase II clinical trial is testing the efficacy of litifilimab, a monoclonal antibody against pDC-specific binding of blood dendritic cell antigen 2 (BDCA2), in systemic [59] and cutaneous [60] lupus erythematosus, where litifilimab is thought to dampen type I IFN production [61,62]. However, the association of pDCs with CD is less well documented. Previous studies have indicated that the circulatory pDC population is significantly decreased in IBD patients with active disease [63], with subsequent research by the same authors showing increased infiltration into the colonic mucosa and mesenteric lymph node (MLN) [64]. This largely corroborates our own observations, as samples were obtained during treatment and the difference between responders and non-responders is, by definition, a difference in inflammation. However, controversy exists on what role pDCs play in the pathogenesis of IBD as experiments have yielded conflicting results. It has been reported that pDCs can aggravate [65], protect [66,67], or are dispensable in the development of experimental IBD [68]. Accordingly, it remains unclear how pDCs might play a role in responsiveness towards VDZ.

Significant differences in expression were observed for the circulating classical monocytes, which presented a more scavenger-like, wound-healing phenotype amongst responders. By contrast, classical monocytes from non-responders appeared to present higher expression of *CFD*, a gene involved in the alternative complement pathway. Complement factor D cleaves factor B forming Bb, thereby activating the complement cascade [69]. The alternative complement pathway is an important component of the innate immune response where it is typically used as first line defense against microbes. Our results would imply that the classical monocytes from non-responders are primed at activating the alternative complement pathway. Such monocytes could potentially be recruited into the intestinal compartment, where they would differentiate into macrophages. Intestinal inflammatory macrophages are one of the few macrophages that are purported to be supplemented by the

circulating monocyte population during inflammatory episodes [70–72]. We show that monocytes indeed present the capability of forming integrin $\alpha_4\beta_7$, based on their gene expression, which corroborates observations by Schleier *et al.* who showed that monocytes indeed present functional integrin $\alpha_4\beta_7$ on their surface, with VDZ abrogating their interactions with MAdCAM-1 *in vitro* [13]. While our observations do not indicate any difference in expression of either ITGA4 or ITGB7, we do note that the classical monocytes, alongside all other myeloid cells, were less abundant among non-responders, which we hypothesize is due to their recruitment out of circulation and into the intestinal compartment.

Taken together, it is evident that response to VDZ during treatment manifests itself at the single-cell level. While the current study provides novel insights into the diagnostic capabilities single-cell transcriptomics for elucidating response to VDZ, we appreciate the shortcomings of this study in terms of the limited sample size as well as the largely associative nature of the observations. More importantly, patient-samples taken during treatment do not hold prognostic value in predicting response to therapy. Future experiments would need to be conducted to validate the differences observed at the level of single-cell transcriptomics in a larger independent cohort to fully understand its utility as biomarker. Furthermore, to disentangle inflammation from VDZ-treatment, samples would need to be included prior to the start of treatment. Moreover, it is imperative to compare our observations with CD patient cohorts treated with other inflammatory-reducing medication to understand which observations VDZ-specific and which observations are inflammation-associated. Such an approach would not only allow for the identification of prognostic biomarkers for VDZ response, but also provide potential targets that might be involved in the manifestation of drug non-response. Taken together, we demonstrate that patients on VDZ treatment present differences in the cellular heterogeneity of PBMCs. Further confirmatory studies are necessary to understand the full potential of the observed differences.

Data Transparency Statement

The data that support the findings of this study are available under controlled access. The raw sequencing data can be found at the European Genome-phenome Archive EGAS00001007328 and EGAS00001007361 for the single-cell RNA-sequencing data and the bulk RNA-sequencing on classical monocytes, respectively. All scripts can be found at https://github.com/ND91/HGPRJ0000008_EPICCD_anti_a4b7_sc.

Funding

This work was partly funded by the Helmsley Foundation as well as local funds from the Department of Human Genetics and the Tytgat Institute for Liver and Intestinal Research,

AmsterdamUMC University of Amsterdam, Amsterdam, Netherlands. The study sponsors had no role in study, design, collection, analysis, or interpretation of data.

Conflicts of interest

The following authors disclose the following within the past 5 years. ALY received speaker fees from Janssen, Johnson & Johnson and was employed by GSK. WJ received speaker fees from Janssen, Johnson & Johnson. GRD received speaker fees from Janssen, Johnson & Johnson. The remaining authors disclose no conflicts.

Acknowledgements

We are thankful to all the participants included in the EPIC-CD study as well as the Core Facility Microscopy and Cytometry and the Core Facility Genomics located at the AmsterdamUMC for their expert assistance in the single-cell RNA-sequencing, mass cytometry, and flow cytometry experiments and analyses.

Legends

Figures

Figure 1. Sampling strategy. Peripheral blood samples were obtained from 4 CD patients that responded to VDZ and 4 CD patients that did not respond to VDZ. Response was defined based the Harvey Bradshaw Index (HBI), C-reactive protein (CRP), fecal calprotectin (fCalpro), and simple-endoscopic score CD (SES-CD). From peripheral blood, peripheral blood mononuclear cells (PBMCs) were isolated which were subsequently used for single-cell RNA-sequencing and mass cytometry by time of flight (CyTOF) using the Chromium controller (10X Genomics) and CyTOF3-Helios systems (Fluidigm), respectively. Created with BioRender.

Figure 2. *ITGA4* is expressed by all cell types. Uniform manifold approximation and projection (UMAP) visualization of the PBMCs from CD patients on VDZ that respond (R; N = 4) and that do not respond (NR; N = 4) colored by the cellular identity as obtained through (A) single-cell RNA-sequencing (scRNAseq) and (B) mass cytometry by time of flight (CyTOF). Visualization of the marker expression used to annotate the PBMCs at the level of (C) gene expression through a dotplot where size and color intensity represent the percentage cells with measurable expression and the median expression, respectively, and (D) protein expression through a heatmap with the color representing the median expression. (E) Scatterplot representing the percentage cell types per sample relative to all PBMCs for scRNAseq on the X-axis and CyTOF on the Y-axis colored by lineage show general

agreement between the scRNAseq and CyTOF experiment. UMAP (left) and boxplot (right) visualization of the gene expression for (F) *ITGA4*, *ITGB7*, as well as (G) the protein expression for integrin α_4 per cell type shows that gene and protein expression of *ITGA4* can be found on all celltypes, whereas *ITGB7* expression is more muted.

Figure 3. T cells present response-associated differences in abundance and expression. Boxplot visualizations of the cell type abundances relative to all measured PBMCs colored by response for (A) scRNAseq and (B) CyTOF. (C) Scatterplot comparing the differences in abundance based on scRNAseq on the X-axis and CyTOF on the Y-axis. Values represent $\log_2$-transformed responder:non-responder ratios per cell type and colors represent the parent lineages of each cell type. (D) Boxplot visualizations of the mean scRNAseq-CyTOF $\log_2$-transformed responder:non-responder ratios shows that T and myeloid cells are significantly more and less abundant amongst non-responders, respectively. Asterisks denote statistical significance using a one-sample t-test against 0. * $p<0.05$; ** $p<0.01$. Boxplot visualizations of the abundance (E) CD8 T central memory (CD8 TCM) in the (left) CyTOF experiment and (right) scRNAseq experiment, (F) mucosal associated invariant T (MAIT) cells, and (G) plasmacytoid dendritic cells (pDC) relative to all PBMCs. *P*-values were calculated using the t-test implementation in speckle::propeller. (H) Dotplot visualization representing the most significant differentially expressed genes, as well as *ITGA4* and *ITGB7* per T cell subset. Size represents statistical significance, transparency the significance threshold, and color whether the gene is upregulated in either responders (green) or non-responders (orange). A notable lower expression of *TNFAIP3* and *NFKBIA* can be observed among non-responders.

Figure 4. Lower abundance of plasmacytoid dendritic cells in PBMCs of non-responding patients.
(A) Flow cytometry strategy used to identify and quantify the HLA-DR$^+$CD14$^-$CD16$^-$CD11c$^-$ CD123$^+$ pDCs where red boxes indicate selected events. (B) Boxplot visualizations of the pDC abundances relative to all measured PBMCs annotated with the *p*-value obtained through t-test. (C) Volcanoplot comparing pDCs from responders with non-responders where the X-axis represents the $\log_2$(fold-change) and the Y-axis the $-\log_{10}$(*p*-value). Highlighted in red are *ITGA4* and *ITGB7*. (D) Boxplot visualizations of the *ITGA4* and *ITGB7* expression in pDCs showing visible but no statistical significant differences between responders and non-responders. *P*-values were calculating using the t-test implementation in speckle::propeller. (E) UMAP visualization of GSE134809 showing (left) the identification strategy of the PTPRC[CD45]$^+$EPCAM$^-$HLA-DRA$^+$ITGAX[CD11c]$^-$ IL3RA[CD123]$^+$CLEC4C[BDCA2]$^+$ pDCs, (right) as highlighted by the red box. (F) Boxplot

visualization of the ileal pDC abundance relative to all immune cells colored by whether they originate from lesions (involved) or outside a lesion (uninvolved) shows that lesional pDCs are more abundant than non-lesional pDCs.

Figure 5. Classical monocytes from non-responding patients present lower expression of cytokine-cytokine signaling. (A) UMAP visualization of the monocytes colored by colored by response as dots (left) and a density plot (right) shows distinct clustering by response for the classical monocytes in particular. (B) Volcanoplot comparing classical monocytes from responders with non-responders where the X-axis represents the $\log_2$(fold change) and the Y-axis the $-\log_{10}$(*p*-value). Statistically significant differences (*p*-value$_{\text{BH-adjusted}}$<0.05) are depicted in black. (C) Boxplot visualizations of *CFD* and *MSR1* expression in classical monocytes colored by response and grouped by patient where each dot represents an individual cell. Boxplot visualizations of (D) *CFD* and *MSR1*, and (E) *ITGA4* and *ITGB7* where the Y-axis represents gene log-transformed (left) normalized pseudobulk expression from our scRNAseq experiment and (right) normalized expression obtained through bulk RNAseq analysis on classical monocytes colored and grouped by response. *P*-values were obtained through Wald test as implemented in DESeq2. (F) Volcanoplot comparing classical monocytes from responders with non-responders where the X-axis represents the normalized enrichment score (NES) and the Y-axis the $-\log_{10}$(*p*-value). Statistically significant differences (*p*-value$_{\text{BH-adjusted}}$<0.05) are depicted in black with pathways of interest highlighted in red. (G) Heatmap visualization genes belonging to the cytokine-cytokine receptor interaction pathway. Values represent the pseudobulk expression per sample, where color is proportion to the level of expression. (H) Dotplot visualization of a receptor/ligand interaction analysis of the differentially expressed cytokines representing ligands and receptors are colored in blue and purple, respectively. Depicted in the dotplot are the binding partners of the cytokines found to be differentially expressed by the classical monocytes for each cell type found in PBMCs. Size of the dots represents statistical significance, transparency the significance threshold, and color whether the gene is upregulated in either responders (green) or non-responders (orange). We find that VEGFA receptor FLT1 is significantly higher expressed among the CD4 naïve and classical monocytes of responders.

Tables

Table 1. Patient characteristics scRNAseq and CyTOF analyses. Overview of the demographics of the included patients.

	Responders (N = 4)	**Non-responders (N = 4)**

Female, N (%)	3 (75)	4 (100)
Age, years, median (IQR)	40 (35-48)	48 (36.5-61.25)
Disease duration, years, median (IQR)	10.5 (7.5-18.5)	7 (4.5-23)
Ethnic background, N (%)		
- Caucasian	3 (75)	1 (25)
C-reactive protein, mg/L, median (IQR)	9.8 (6.5-14.35)	2.2 (1.4-2.8)
Faecal calprotectin, µg/g, median (IQR)	329 (168-850)	263 (189-305)
Disease location, n (%)		
- Ileal disease (L1)	3 (75)	1 (25)
- Colonic disease (L2)	-	-
- Ileocolonic disease (L3)	1 (25)	3 (75)
Disease behavior, N (%)		
- Non structuring/penetrating (B1)	1 (25)	2 (50)
- Stricturing (B2)	2 (50)	2 (50)
- Penetrating (B3)	1 (25)	-
- Perianal disease (p)	1 (25)	-
Previous IBD-related surgery, N (%)	2 (50)	1 (25)
Concomitant medication, N (%)		
- Immunomodulators	-	-
- Prednisone	-	-
Previous biological treatment, N (%)		
- Immunomodulators	3 (75)	1 (25)
- Anti-TNF (ADA or IFX)	1 (25)	3 (75)
Smoking, N (%)		
- Never	1 (25)	1 (25)
- Active	-	3 (75)
- Former	3 (75)	-

Supplementary Tables

Supplemental Table 1. Marker panel mass cytometry. The cell-surface exposed markers assayed in the mass cytometry experiment annotated by the metal, target protein, alternative names, uniport identifier, and notes.

Supplemental Table 2. Marker panel flow cytometry. The cell-surface exposed markers assayed in the flow cytometry experiment alongside the antibody and clone.

Supplemental Table 3. PBMC differential abundance analysis. Results of the differential abundance analysis on the major lineages as conducted using the propeller function in speckle. Columns represent the cell type, the mean proportion for all samples (“BaselineProp.Freq”), non-responders only (“PropMean.Non.responder”), and responders only (“PropMean.Responder”), the ratio responder/non-responder (“PropRatio”), the

associated T statistic ("Tstatistic") as well as the *p*-values ("P.Value" and "FDR"). Tabs separate the results from scRNAseq and CyTOF analyses.

Supplemental Table 4. T cell scRNAseq pseudobulk differential gene expression analysis. Results of the differential expression analysis performed on PDCs using DESeq2. Columns represent the gene, the average expression ("baseMean"), the $\log_2$(fold change) ("log2FoldChange"), the associated standard error ("lfcSE"), the Wald statistic ("stat") as well as the *p*-values ("pvalue" and "padj"). Each tab represents a different T cell subset.

Supplemental Table 5. pDC scRNAseq pseudobulk differential gene expression analysis. Results of the differential expression analysis performed on PDCs using DESeq2. Columns represent the gene, the average expression ("baseMean"), the $\log_2$(fold change) ("log2FoldChange"), the associated standard error ("lfcSE"), the Wald statistic ("stat") as well as the *p*-values ("pvalue" and "padj").

Supplemental Table 6. Classical monocytes scRNAseq pseudobulk differential gene expression analysis. Results of the differential expression analysis performed on classical monocytes using DESeq2. Columns represent the gene, the average expression ("baseMean"), the $\log_2$(fold change) ("log2FoldChange"), the associated standard error ("lfcSE"), the Wald statistic ("stat") as well as the *p*-values ("pvalue" and "padj").

Supplemental Table 7. Classical monocytes bulk RNAseq gene expression analysis. Results of the differential expression analysis performed on classical monocytes using DESeq2. Columns represent the gene and Ensembl ID, the average expression ("baseMean"), the $\log_2$(fold change) ("log2FoldChange"), the associated standard error ("lfcSE"), the Wald statistic ("stat") as well as the *p*-values ("pvalue" and "padj").

Supplemental Table 8. Classical monocytes scRNAseq pseudobulk KEGG gene set enrichment analysis. Gene set enrichment analysis as performed by fgsea. Columns represent the gene set ("Pathway"), the *p*-values ("pvalue" and "FDR"), the $\log_2$ standard error ("log2err"), the enrichment score ("ES"), the normalized enrichment score ("NES"), and the total number of genes in the gene set ("size").

References

1. Li Yim AYF. *Towards the identification of Crohn's disease-associated epigenetic biomarkers in leukocytes. A potential role in personalized diagnostics and treatment*. Amsterdam: Universiteit van Amsterdam; 2022.

2. Sandborn WJ, Feagan BG, Rutgeerts P, et al. Vedolizumab as Induction and Maintenance Therapy for Crohn's Disease. https://doi.org/101056/NEJMoa1215739 2013;369:711–721. Available at: https://www.nejm.org/doi/10.1056/NEJMoa1215739 [Accessed January 31, 2023].

3. Meenan J, Spaans J, Grool TA, et al. Altered expression of α4β7, a gut homing integrin, by circulating and mucosal T cells in colonic mucosal inflammation. Gut 1997.

4. Gorfu G, Rivera-Nieves J, Ley K. *Role of 7 Integrins in Intestinal Lymphocyte Homing and Retention*. 2009.

5. Yang Y, Cardarelli PM, Lehnert K, et al. LPAM-1 (integrin α4β7)-ligand binding: Overlapping binding sites recognizing VCAM-1, MAdCAM-1 and CS-1 are blocked by fibrinogen, a fibronectin-like polymer and RGD-like cyclic peptides. Eur J Immunol 1998.

6. Berlin C, Bargatze RF, Campbell JJ, et al. *a4 Integrins Mediate Lymphocyte Attachment and Rolling under Physiologic Flow*. 1995.

7. Hynes RO. Integrins: bidirectional, allosteric signaling machines. Cell 2002;110:673–687.

8. Soler D, Chapman T, Yang LL, et al. The binding specificity and selective antagonism of vedolizumab, an anti-α4β7 integrin therapeutic antibody in development for inflammatory bowel diseases. Journal of Pharmacology and Experimental Therapeutics 2009;330:864–875.

9. Arijs I, Hertogh G De, Lemmens B, et al. Effect of vedolizumab (anti-α4β7-integrin) therapy on histological healing and mucosal gene expression in patients with UC. Gut 2018;67:43–52. Available at: http://gut.bmj.com/lookup/doi/10.1136/gutjnl-2016-312293 [Accessed June 9, 2020].

10. Lord JD, Long SA, Shows DM, et al. Circulating integrin alpha4/beta7+ lymphocytes targeted by vedolizumab have a pro-inflammatory phenotype. Clinical Immunology 2018;193:24–32.

11. Habtezion A, Nguyen LP, Hadeiba H, et al. Leukocyte Trafficking to the Small Intestine and Colon. Gastroenterology 2016;150:340–354.

12. Zeissig S, Rosati E, Dowds CM, et al. Vedolizumab is associated with changes in innate rather than adaptive immunity in patients with inflammatory bowel disease. Gut 2019;68:25–39. Available at: http://www.ncbi.nlm.nih.gov/pubmed/29730603 [Accessed November 12, 2019].

13. Schleier L, Wiendl M, Heidbreder K, et al. Non-classical monocyte homing to the gut via α4β7 integrin mediates macrophage-dependent intestinal wound healing. Gut 2020;69:252–263.

14. Canales-Herrerias P, Uzzan M, Seki A, et al. Gut-associated lymphoid tissue attrition associates with response to anti-α4β7 therapy in ulcerative colitis. bioRxiv 2023:2023.01.19.524731. Available at: https://www.biorxiv.org/content/10.1101/2023.01.19.524731v1 [Accessed May 7, 2023].

15. Dulai PS, Singh S, Jiang X, et al. The real-world effectiveness and safety of vedolizumab for moderate-severe Crohn's disease: Results from the US VICTORY consortium. American Journal of Gastroenterology 2016.

16. Ungar B, Kopylov U, Yavzori M, et al. Association of Vedolizumab Level, Anti-Drug Antibodies, and α4β7 Occupancy With Response in Patients With Inflammatory Bowel Diseases. Clin Gastroenterol Hepatol 2018;16:697-705.e7. Available at: https://pubmed.ncbi.nlm.nih.gov/29223444/ [Accessed January 31, 2023].

17. Perry C, Fischer K, Elmoursi A, et al. Vedolizumab Dose Escalation Improves Therapeutic Response in a Subset of Patients with Ulcerative Colitis. Dig Dis Sci 2021;66:2051–2058. Available at: https://link.springer.com/article/10.1007/s10620-020-06486-x [Accessed May 7, 2023].

18. Peyrin-Biroulet L, Danese S, Argollo M, et al. *Loss of Response to Vedolizumab and Ability of Dose Intensification to Restore Response in Patients With Crohn's Disease or Ulcerative Colitis: A Systematic Review and Meta-analysis*. W.B. Saunders; 2019:838-846.e2. Available at: https://www.sciencedirect.com/science/article/pii/S1542356518306360?via%3Dihub [Accessed October 6, 2019].

19. Joustra V, Li Yim A, Hageman I, et al. Highly stable epigenome-wide peripheral blood DNA methylation signatures accurately predict endoscopic response to adalimumab, vedolizumab and ustekinumab in Crohn's disease patients: The EPIC-CD study. In: *Journal of Crohn's and Colitis*.Vol 17. Copenhagen; 2023:i6–i8. Available at: https://doi.org/10.1093/ecco-jcc/jjac190.0003.

20. Stoeckius M, Zheng S, Houck-Loomis B, et al. Cell Hashing with barcoded antibodies enables multiplexing and doublet detection for single cell genomics. Genome Biol 2018;19:224. Available at: https://genomebiology.biomedcentral.com/articles/10.1186/s13059-018-1603-1 [Accessed May 30, 2019].

21. Butler A, Hoffman P, Smibert P, et al. Integrating single-cell transcriptomic data across different conditions, technologies, and species. Nat Biotechnol 2018;36:411–420. Available at: https://www.ncbi.nlm.nih.gov/pubmed/29608179.

22. Luecken MD, Theis FJ. Current best practices in single-cell RNA-seq analysis: a tutorial. Mol Syst Biol 2019;15:e8746. Available at: http://msb.embopress.org/lookup/doi/10.15252/msb.20188746.

23. Hafemeister C, Satija R. Normalization and variance stabilization of single-cell RNA-seq data using regularized negative binomial regression. Genome Biol 2019;20:296. Available at: https://genomebiology.biomedcentral.com/articles/10.1186/s13059-019-1874-1 [Accessed October 27, 2020].

24. Stuart T, Butler A, Hoffman P, et al. Comprehensive Integration of Single-Cell Data. Cell 2019;177:1888-1902.e21.

25. Hao Y, Hao S, Andersen-Nissen E, et al. Integrated analysis of multimodal single-cell data. Cell 2021;184:3573-3587.e29.

26. Franzén O, Gan LM, Björkegren JLM. PanglaoDB: A web server for exploration of mouse and human single-cell RNA sequencing data. Database 2019;2019.

27. Phipson B, Sim CB, Porrello ER, et al. propeller: testing for differences in cell type proportions in single cell data. Bioinformatics 2022;38:4720–4726. Available at: https://academic.oup.com/bioinformatics/article/38/20/4720/6675456 [Accessed May 7, 2023].

28. Squair JW, Gautier M, Kathe C, et al. Confronting false discoveries in single-cell differential expression. Nature Communications 2021 12:1 2021;12:1–15. Available at: https://www.nature.com/articles/s41467-021-25960-2 [Accessed August 9, 2022].

29. Love MI, Huber W, Anders S. Moderated estimation of fold change and dispersion for RNA-seq data with DESeq2. Genome Biol 2014;15:550. Available at: http://genomebiology.biomedcentral.com/articles/10.1186/s13059-014-0550-8.

30. Sergushichev AA. An algorithm for fast preranked gene set enrichment analysis using cumulative statistic calculation. bioRxiv 2016:060012. Available at: https://www.biorxiv.org/content/10.1101/060012v1 [Accessed May 19, 2019].

31. Kanehisa M, Sato Y, Kawashima M, et al. KEGG as a reference resource for gene and protein annotation. Nucleic Acids Res 2016;44:D457–D462.

32. Andrews S. FastQC: a quality control tool for high throughput sequence data. Available at: http://www.bioinformatics.babraham.ac.uk/projects/fastqc.

33. Ewels P, Magnusson M, Lundin S, et al. MultiQC: summarize analysis results for multiple tools and samples in a single report. Bioinformatics 2016;32:3047–3048. Available at: https://www.ncbi.nlm.nih.gov/pubmed/27312411.

34. Cunningham F, Allen JE, Allen J, et al. Ensembl 2022. Nucleic Acids Res 2022;50:D988–D995. Available at: https://academic.oup.com/nar/article/50/D1/D988/6430486 [Accessed May 7, 2023].

35. Li H, Handsaker B, Wysoker A, et al. The Sequence Alignment/Map format and SAMtools. Bioinformatics 2009;25:2078–2079. Available at: internal-pdf://0894036185/pmcid-PMC3348047.ris.

36. Liao Y, Smyth GK, Shi W. The Subread aligner: fast, accurate and scalable read mapping by seed-and-vote. Nucleic Acids Res 2013;41:e108.

37. Gentleman RC, Carey VJ, Bates DM, et al. Bioconductor: open software development for computational biology and bioinformatics. Genome Biol 2004;5:R80. Available at: https://doi.org/10.1186/gb-2004-5-10-r80.

38. R Development Core Team. *R: A language and environment for statistical computing*. Vienna, Austria: R Foundation for Statistical Computing; 2008. Available at: http://www.r-project.org/.

39. Martin JC, Chang C, Boschetti G, et al. Single-Cell Analysis of Crohn's Disease Lesions Identifies a Pathogenic Cellular Module Associated with Resistance to Anti-TNF Therapy. Cell 2019;178:1493-1508.e20. Available at:

https://www.sciencedirect.com/science/article/pii/S0092867419308967 [Accessed October 16, 2019].

40. Pelus LM, Fukuda S. Peripheral blood stem cell mobilization: The CXCR2 ligand GROβ rapidly mobilizes hematopoietic stem cells with enhanced engraftment properties. Exp Hematol 2006;34:1010–1020.

41. Wolpe SD, Sherry B, Juers D, et al. Identification and characterization of macrophage inflammatory protein 2. Proceedings of the National Academy of Sciences 1989;86:612–616. Available at: https://www.pnas.org/doi/abs/10.1073/pnas.86.2.612 [Accessed May 7, 2023].

42. Li Y, Zheng Y, Yang L, et al. Chemokines CCL14 and CCL3 Facilitate Monocytes/Macrophage Infiltration in Multiple Myeloma Bone Marrow. Blood 2014;124:3380–3380. Available at: https://ashpublications.org/blood/article/124/21/3380/97633/Chemokines-CCL14-and-CCL3-Facilitate-Monocytes [Accessed May 7, 2023].

43. Kapellos TS, Bonaguro L, Gemünd I, et al. Human monocyte subsets and phenotypes in major chronic inflammatory diseases. Front Immunol 2019;10:2035.

44. Zhao X, Gu M, Xu X, et al. CCL3/CCR1 mediates CD14+CD16− circulating monocyte recruitment in knee osteoarthritis progression. Osteoarthritis Cartilage 2020;28:613–625. Available at: http://www.oarsijournal.com/article/S1063458420300352/fulltext [Accessed May 7, 2023].

45. Menten P, Wuyts A, Damme J Van. Macrophage inflammatory protein-1. Cytokine Growth Factor Rev 2002;13:455–481.

46. Sindhu S, Kochumon S, Shenouda S, et al. The Cooperative Induction of CCL4 in Human Monocytic Cells by TNF-α and Palmitate Requires MyD88 and Involves MAPK/NF-κB Signaling Pathways. International Journal of Molecular Sciences 2019, Vol 20, Page 4658 2019;20:4658. Available at: https://www.mdpi.com/1422-0067/20/18/4658/htm [Accessed May 7, 2023].

47. Canning P, Ruan Q, Schwerd T, et al. Inflammatory Signaling by NOD-RIPK2 Is Inhibited by Clinically Relevant Type II Kinase Inhibitors. Chem Biol 2015;22:1174–1184.

48. Gudgeon J, Marín-Rubio JL, Trost M. The role of macrophage scavenger receptor 1 (MSR1) in inflammatory disorders and cancer. Front Immunol 2022;13:6173.

49. Wang XF, En-Zhou, Li DJ, et al. VSTM1 regulates monocyte/macrophage function via the NF-κB signaling pathway. Open Medicine (Poland) 2021;16:1513–1524. Available at: https://www.degruyter.com/document/doi/10.1515/med-2021-0353/html [Accessed May 7, 2023].

50. Reizis B, Idoyaga J, Dalod M, et al. Reclassification of plasmacytoid dendritic cells as innate lymphocytes is premature. Nature Reviews Immunology 2023 23:5 2023;23:336–337. Available at: https://www.nature.com/articles/s41577-023-00864-y [Accessed May 25, 2023].

51. Ziegler-Heitbrock L, Ohteki T, Ginhoux F, et al. Reclassifying plasmacytoid dendritic cells as innate lymphocytes. Nature Reviews Immunology 2022 23:1 2022;23:1–2. Available at: https://www.nature.com/articles/s41577-022-00806-0 [Accessed January 21, 2023].

52. Musumeci A, Lutz K, Winheim E, et al. What makes a PDC: Recent advances in understanding plasmacytoid DC development and heterogeneity. Front Immunol 2019;10:1222.

53. Reizis B. Plasmacytoid Dendritic Cells: Development, Regulation, and Function. Immunity 2019;50:37–50. Available at: http://www.cell.com/article/S1074761318305752/fulltext [Accessed December 17, 2022].

54. Ye Y, Gaugler B, Mohty M, et al. Plasmacytoid dendritic cell biology and its role in immune-mediated diseases. Clin Transl Immunology 2020;9:e1139. Available at: https://onlinelibrary.wiley.com/doi/full/10.1002/cti2.1139 [Accessed October 16, 2022].

55. Bencze D, Fekete T, Pázmándi K. Type I Interferon Production of Plasmacytoid Dendritic Cells under Control. International Journal of Molecular Sciences 2021, Vol 22, Page 4190 2021;22:4190. Available at: https://www.mdpi.com/1422-0067/22/8/4190/htm [Accessed May 12, 2023].

56. Asselin-Paturel C, Trinchieri G. Production of type I interferons plasmacytoid dendritic cells and beyond. Journal of Experimental Medicine 2005;202:461–465. Available at: www.jem.org/cgi/doi/10.1084/jem.20051395 [Accessed May 12, 2023].

57. Colonna M, Trinchieri G, Liu YJ. Plasmacytoid dendritic cells in immunity. Nature Immunology 2004 5:12 2004;5:1219–1226. Available at: https://www.nature.com/articles/ni1141 [Accessed May 12, 2023].

58. Getz GS. Bridging the innate and adaptive immune systems. J Lipid Res 2005;46:619–622. Available at: http://www.jlr.org/article/S002222752033995X/fulltext [Accessed May 12, 2023].

59. Huang X, Dorta-Estremera S, Yao Y, et al. Predominant role of plasmacytoid dendritic cells in stimulating systemic autoimmunity. Front Immunol 2015;6:526.

60. Vermi W, Lonardi S, Morassi M, et al. Cutaneous distribution of plasmacytoid dendritic cells in lupus erythematosus. Selective tropism at the site of epithelial apoptotic damage. Immunobiology 2009;214:877–886.

61. Werth VP, Furie RA, Romero-Diaz J, et al. Trial of Anti-BDCA2 Antibody Litifilimab for Cutaneous Lupus Erythematosus. New England Journal of Medicine 2022;387:321–331. Available at: https://www.nejm.org/doi/full/10.1056/NEJMoa2118024 [Accessed May 25, 2023].

62. Furie RA, Vollenhoven RF van, Kalunian K, et al. Trial of Anti-BDCA2 Antibody Litifilimab for Systemic Lupus Erythematosus. New England Journal of Medicine 2022;387:894–904.

63. Baumgart DC, Metzke D, Schmitz J, et al. Patients with active inflammatory bowel disease lack immature peripheral blood plasmacytoid and myeloid dendritic cells. Gut 2005;54:228–236. Available at: www.gutjnl.com.

64. Baumgart DC, Metzke D, Guckelberger O, et al. Aberrant plasmacytoid dendritic cell distribution and function in patients with Crohn's disease and ulcerative colitis. Clin Exp Immunol 2011;166:46–54.

65. Arimura K, Takagi H, Uto T, et al. Crucial role of plasmacytoid dendritic cells in the development of acute colitis through the regulation of intestinal inflammation. Mucosal Immunology 2017 10:4 2016;10:957–970. Available at: https://www.nature.com/articles/mi201696 [Accessed May 25, 2023].

66. Mizuno S, Kanai T, Mikami Y, et al. CCR9+ plasmacytoid dendritic cells in the small intestine suppress development of intestinal inflammation in mice. Immunol Lett 2012;146:64–69.

67. Rahman T, Brown AS, Hartland EL, et al. Plasmacytoid dendritic cells provide protection against bacterial-induced colitis. Front Immunol 2019;10:608.

68. Sawai CM, Serpas L, Neto AG, et al. Plasmacytoid dendritic cells are largely dispensable for the pathogenesis of experimental inflammatory bowel disease. Front Immunol 2018;9:2475.

69. Barratt J, Weitz I. Complement Factor D as a Strategic Target for Regulating the Alternative Complement Pathway. Front Immunol 2021;12:3595.

70. Bain CC, Scott CL, Uronen-Hansson H, et al. Resident and pro-inflammatory macrophages in the colon represent alternative context-dependent fates of the same Ly6Chi monocyte precursors. Mucosal Immunol 2013;6:498–510.

71. Bain CC, Schridde A. Origin, Differentiation, and Function of Intestinal Macrophages. Front Immunol 2018;9:2733.

72. Bain CC, Mowat AM. The monocyte-macrophage axis in the intestine. Cell Immunol 2014;291:41–48.

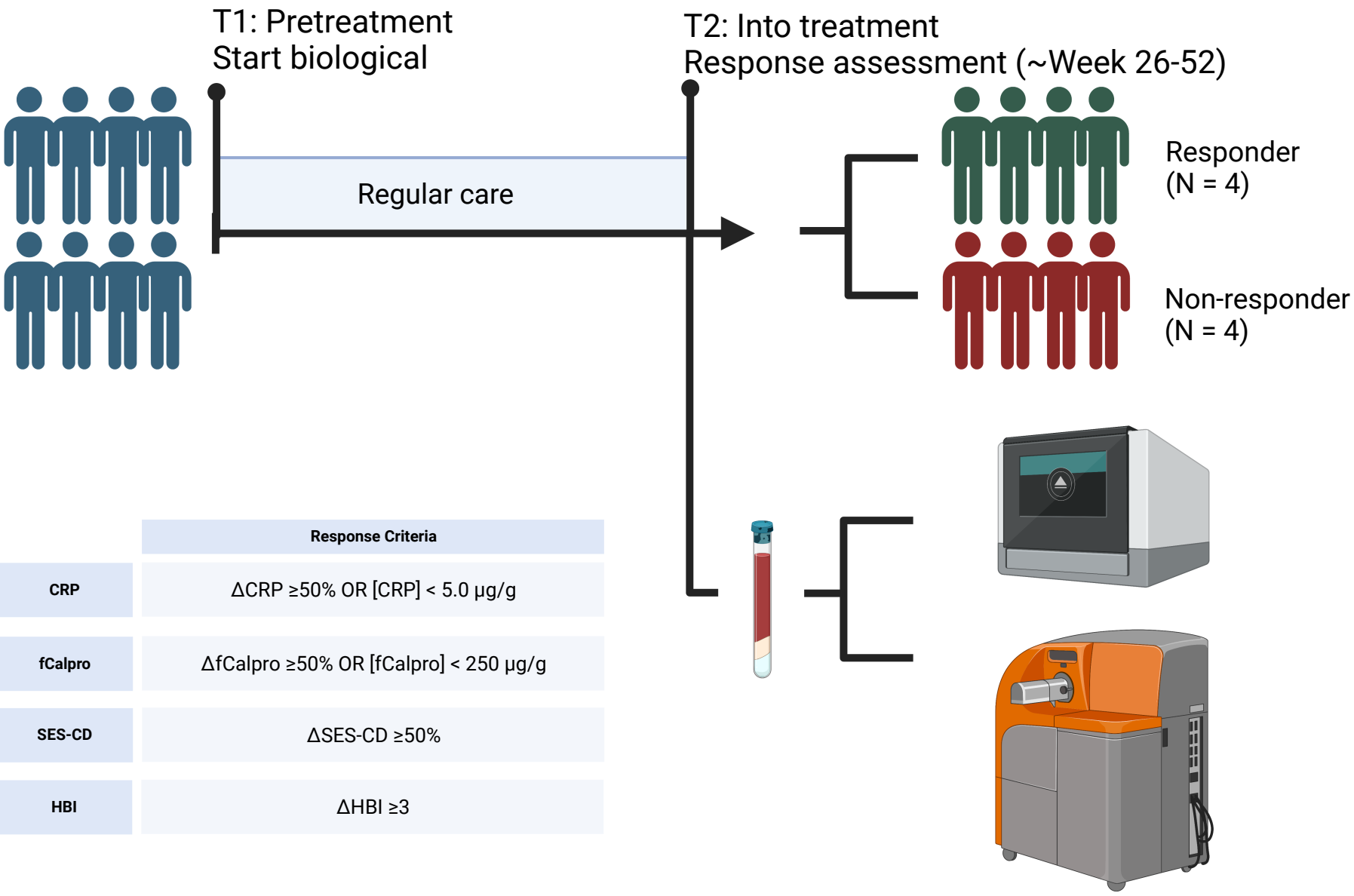

	Response Criteria
CRP	ΔCRP ≥50% OR [CRP] < 5.0 µg/g
fCalpro	ΔfCalpro ≥50% OR [fCalpro] < 250 µg/g
SES-CD	ΔSES-CD ≥50%
HBI	ΔHBI ≥3

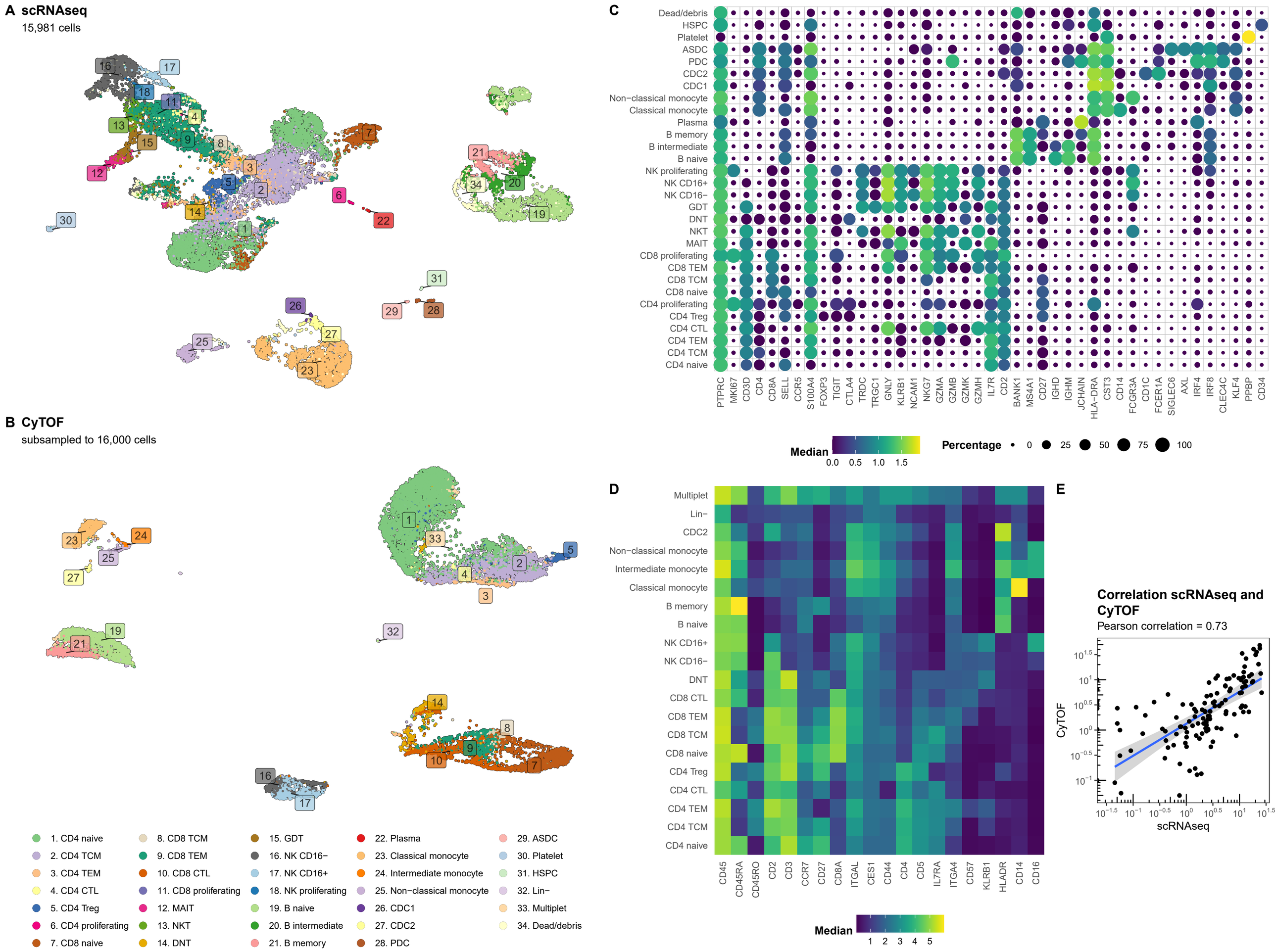
A scRNAseq
15,981 cells
B CyTOF
subsampled to 16,000 cells
C
Dead/debris
HSPC
Platelet
ASDC
PDC
CDC2
CDC1
Non−classical monocyte
Classical monocyte
Plasma
B memory
B intermediate
B naive
NK proliferating
NK CD16+
NK CD16−
GDT
DNT
NKT
MAIT
CD8 proliferating
CD8 TEM
CD8 TCM
CD8 naive
CD4 proliferating
CD4 Treg
CD4 CTL
CD4 TEM
CD4 TCM
CD4 naive
PTPRC MKI67 CD3D CD4 CD8A SELL CCR5 S100A4 FOXP3 TIGIT CTLA4 TRDC TRGC1 GNLY KLRB1 NCAM1 NKG7 GZMA GZMB GZMK GZMH IL7R CD2 BANK1 MS4A1 CD27 IGHD IGHM JCHAIN HLA−DRA CST3 CD14 FCGR3A CD1C FCER1A SIGLEC6 AXL IRF4 IRF8 CLEC4C KLF4 PPBP CD34
Median 0.0 0.5 1.0 1.5
Percentage 0 25 50 75 100
D
Multiplet
Lin−
CDC2
Non−classical monocyte
Intermediate monocyte
Classical monocyte
B memory
B naive
NK CD16+
NK CD16−
DNT
CD8 CTL
CD8 TEM
CD8 TCM
CD8 naive
CD4 Treg
CD4 CTL
CD4 TEM
CD4 TCM
CD4 naive
CD45 CD45RA CD45RO CD2 CD3 CCR7 CD27 CD8A ITGAL CES1 CD44 CD4 CD5 IL7RA ITGA4 CD57 KLRB1 HLADR CD14 CD16
Median 1 2 3 4 5
E
Correlation scRNAseq and CyTOF
Pearson correlation = 0.73
CyTOF
scRNAseq
1. CD4 naive
2. CD4 TCM
3. CD4 TEM
4. CD4 CTL
5. CD4 Treg
6. CD4 proliferating
7. CD8 naive
8. CD8 TCM
9. CD8 TEM
10. CD8 CTL
11. CD8 proliferating
12. MAIT
13. NKT
14. DNT
15. GDT
16. NK CD16−
17. NK CD16+
18. NK proliferating
19. B naive
20. B intermediate
21. B memory
22. Plasma
23. Classical monocyte
24. Intermediate monocyte
25. Non−classical monocyte
26. CDC1
27. CDC2
28. PDC
29. ASDC
30. Platelet
31. HSPC
32. Lin−
33. Multiplet
34. Dead/debris
F
scRNAseq: ITGA4
scRNAseq: ITGB7
Expression
2
4
6
nUMIs
G
Mass cytometry: integrin α4
CD4 naive CD4 TCM CD4 TEM CD4 CTL CD4 Treg CD4 proliferating CD8 naive CD8 TCM CD8 TEM CD8 CTL CD8 proliferating MAIT NKT DNT GDT NK CD16− NK CD16+ NK proliferating B naive B intermediate B memory Plasma Classical monocyte Intermediate monocyte Non−classical monocyte CDC1 CDC2 PDC ASDC Platelet HSPC Lin− Multiplet Dead/debris

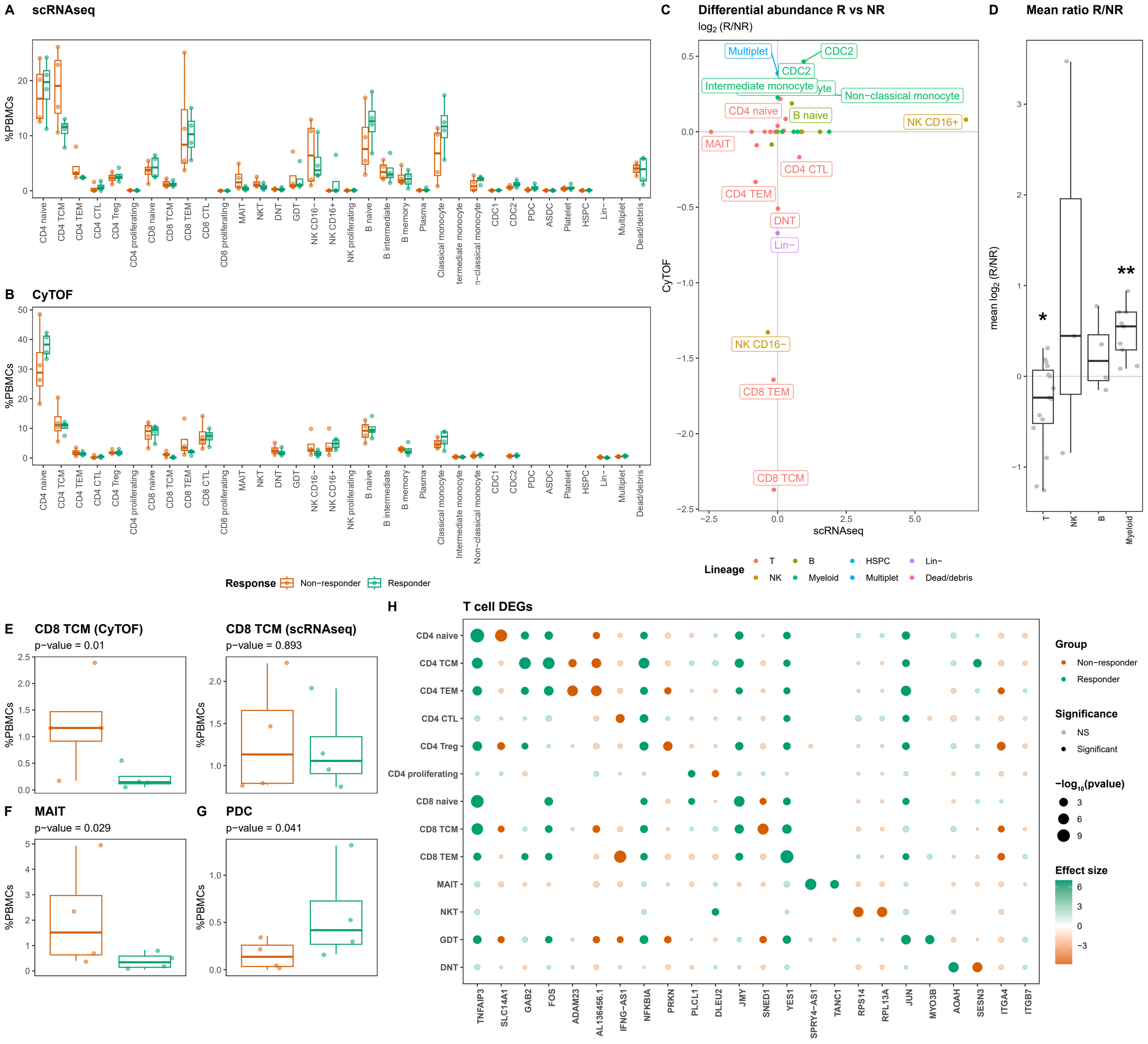
A scRNAseq
%PBMCs
CD4 naive
CD4 TCM
CD4 TEM
CD4 CTL
CD4 Treg
CD4 proliferating
CD8 naive
CD8 TCM
CD8 TEM
CD8 CTL
CD8 proliferating
MAIT
NKT
DNT
GDT
NK CD16−
NK CD16+
NK proliferating
B naive
B intermediate
B memory
Plasma
Classical monocyte
Intermediate monocyte
Non−classical monocyte
CDC1
CDC2
PDC
ASDC
Platelet
HSPC
Lin−
Multiplet
Dead/debris
B CyTOF
Response
Non−responder
Responder
C Differential abundance R vs NR
log2 (R/NR)
CyTOF
scRNAseq
Multiplet
CDC2
Intermediate monocyte
Non−classical monocyte
CD4 naive
B naive
NK CD16+
MAIT
CD4 CTL
CD4 TEM
DNT
Lin−
NK CD16−
CD8 TEM
CD8 TCM
Lineage
T
NK
B
Myeloid
HSPC
Multiplet
Lin−
Dead/debris
D Mean ratio R/NR
mean log2 (R/NR)
T
NK
B
Myeloid
E CD8 TCM (CyTOF)
p−value = 0.01
CD8 TCM (scRNAseq)
p−value = 0.893
F MAIT
p−value = 0.029
G PDC
p−value = 0.041
H T cell DEGs
Group
Non−responder
Responder
Significance
NS
Significant
−log10(pvalue)
Effect size
TNFAIP3
SLC14A1
GAB2
FOS
ADAM23
AL136456.1
IFNG−AS1
NFKBIA
PRKN
PLCL1
DLEU2
JMY
SNED1
YES1
SPRY4−AS1
TANC1
RPS14
RPL13A
JUN
MYO3B
AOAH
SESN3
ITGA4
ITGB7

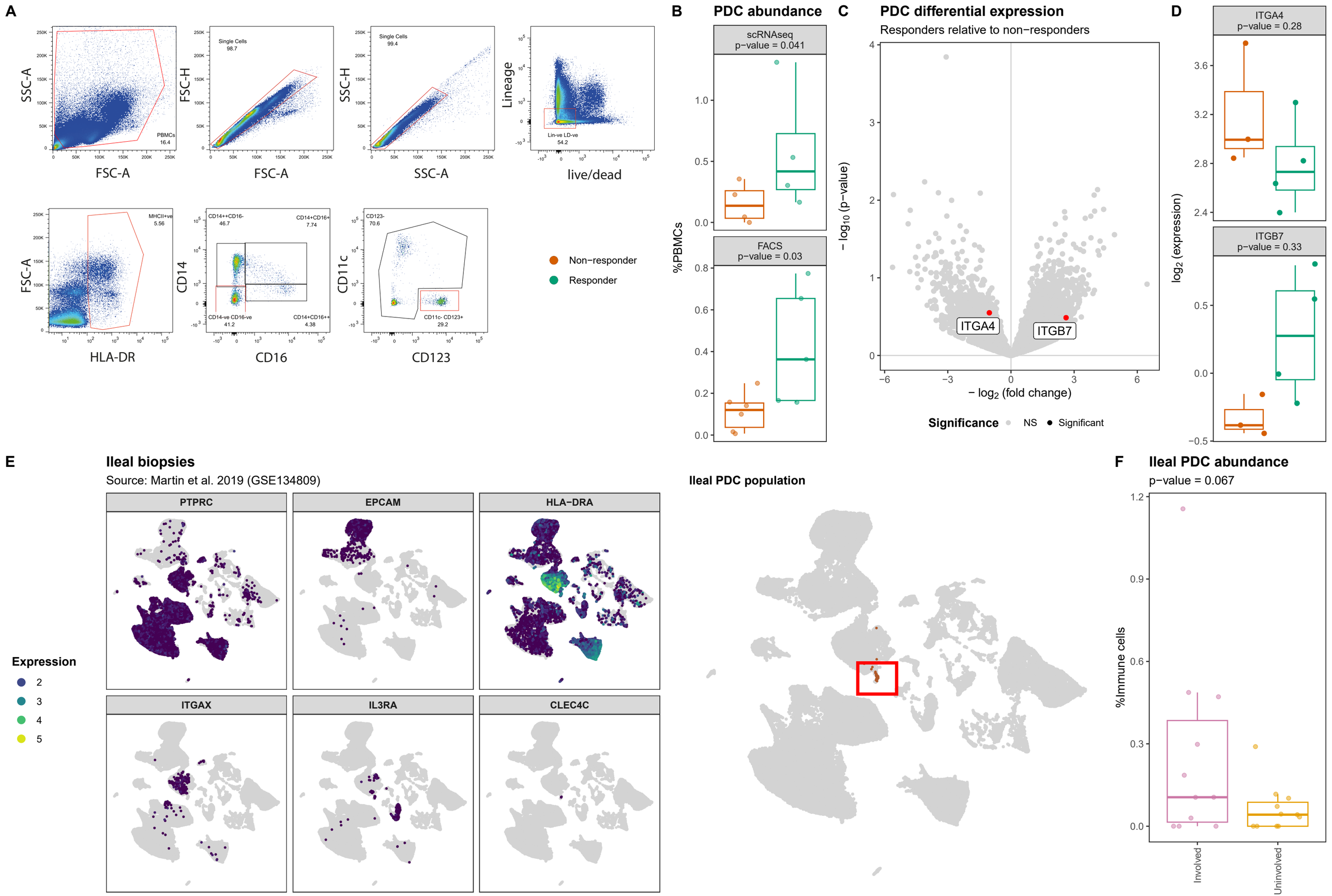
A
SSC-A
FSC-A
PBMCs
16.4
FSC-H
Single Cells
98.7
SSC-H
Single Cells
99.4
Lineage
live/dead
Lin-ve LD-ve
54.2
HLA-DR
MHCII+ve
5.56
CD14
CD16
CD14++CD16-
46.7
CD14+CD16+
7.74
CD14-ve CD16-ve
41.2
CD14+CD16++
4.38
CD11c
CD123
CD123-
70.6
CD11c- CD123+
29.2
Non−responder
Responder
B
PDC abundance
scRNAseq
p−value = 0.041
FACS
p−value = 0.03
%PBMCs
C
PDC differential expression
Responders relative to non−responders
− log10 (p−value)
− log2 (fold change)
ITGA4
ITGB7
Significance
NS
Significant
D
ITGA4
p−value = 0.28
ITGB7
p−value = 0.33
log2 (expression)
E
Ileal biopsies
Source: Martin et al. 2019 (GSE134809)
PTPRC
EPCAM
HLA−DRA
ITGAX
IL3RA
CLEC4C
Expression
2
3
4
5
Ileal PDC population
F
Ileal PDC abundance
p−value = 0.067
%Immune cells
Involved
Uninvolved

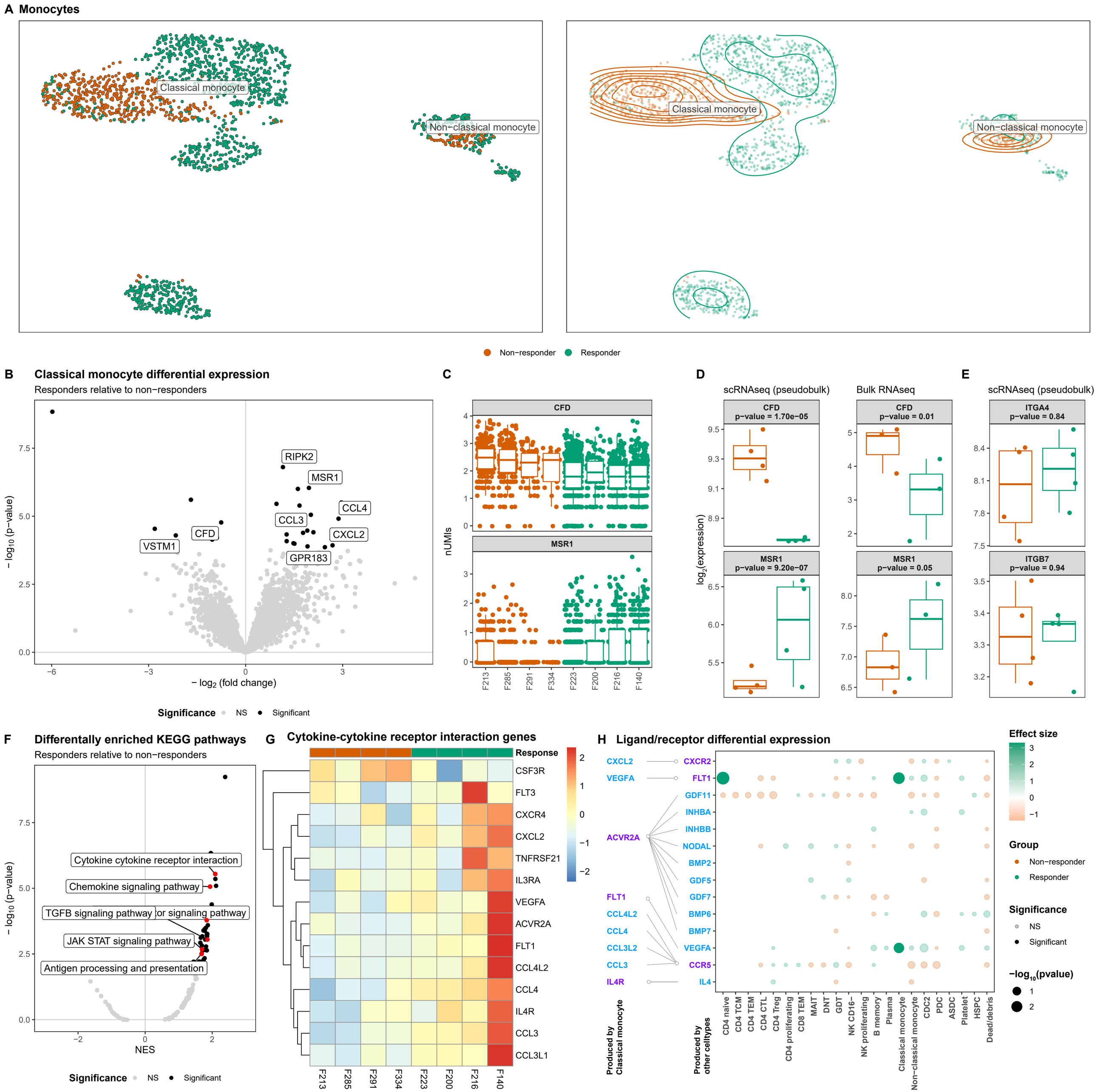
A Monocytes
Classical monocyte
Non−classical monocyte
Non−responder
Responder
B Classical monocyte differential expression
Responders relative to non−responders
RIPK2
MSR1
CCL4
CCL3
CXCL2
CFD
VSTM1
GPR183
− log10 (p−value)
− log2 (fold change)
Significance NS Significant
C
CFD
MSR1
nUMIs
F213 F285 F291 F334 F223 F200 F216 F140
D
scRNAseq (pseudobulk)
Bulk RNAseq
CFD p−value = 1.70e−05
CFD p−value = 0.01
MSR1 p−value = 9.20e−07
MSR1 p−value = 0.05
log2(expression)
E
scRNAseq (pseudobulk)
ITGA4 p−value = 0.84
ITGB7 p−value = 0.94
F Differentially enriched KEGG pathways
Responders relative to non−responders
Cytokine cytokine receptor interaction
Chemokine signaling pathway
TGFB signaling pathway
JAK STAT signaling pathway
Antigen processing and presentation
− log10 (p−value)
NES
Significance NS Significant
G Cytokine-cytokine receptor interaction genes
Response
CSF3R
FLT3
CXCR4
CXCL2
TNFRSF21
IL3RA
VEGFA
ACVR2A
FLT1
CCL4L2
CCL4
IL4R
CCL3
CCL3L1
F213 F285 F291 F334 F223 F200 F216 F140
H Ligand/receptor differential expression
CXCL2
VEGFA
ACVR2A
FLT1
CCL4L2
CCL4
CCL3L2
CCL3
IL4R
CXCR2
FLT1
GDF11
INHBA
INHBB
NODAL
BMP2
GDF5
GDF7
BMP6
BMP7
VEGFA
CCR5
IL4
Produced by Classical monocyte
Produced by other celltypes
CD4 naive
CD4 TCM
CD4 TEM
CD4 CTL
CD4 Treg
CD4 proliferating
CD8 TEM
MAIT
DNT
GDT
NK CD16−
NK proliferating
B memory
Plasma
Classical monocyte
Non−classical monocyte
CDC2
PDC
ASDC
Platelet
HSPC
Dead/debris
Effect size
Group
Non−responder
Responder
Significance
NS
Significant
−log10(pvalue)